Chapter 3
Integrated Kinetic Energy in North Atlantic Tropical Cyclones: Climatology, Analysis, and Seasonal Applications

Michael E. Kozar and Vasubandhu Misra

Abstract Integrated Kinetic Energy (IKE) is a recently developed metric that measures the destructive potential of tropical cyclones (TCs) by integrating the square of the surface winds across these powerful storms. In this chapter, the previous literature is reviewed to provide insights on the factors that make IKE a desirable metric. IKE complements existing scales and metrics by considering a TC's entire wind field, in lieu of just focusing on the maximum intensity of a storm. Using a dataset of six-hourly IKE estimates for two decades of North Atlantic TC activity, the climatology of IKE in individual storms is explored, with emphasis on seasonal and spatial variability. The driving mechanisms for IKE variability during the lifetime of a TC are also reviewed to determine which environmental and storm-scale features promote IKE growth. The historical record of IKE can also be aggregated to a seasonal metric, called Track Integrated Kinetic Energy (TIKE), which is shown to offer a comprehensive overview of seasonal TC activity and can be used to explore interannual TC variability over the last two to three decades.

Keywords Atlantic hurricanes · Integrated kinetic energy · Tropical cyclone structure · Statistical-dynamical analysis · Seasonal activity

M. E. Kozar (✉)
Risk Management Solutions (RMS), Tallahassee, FL, USA
e-mail: Michael.Kozar@rms.com

V. Misra
Center for Ocean-Atmospheric Prediction Studies, Florida State University, Tallahassee, FL, USA

Department of Earth, Ocean and Atmospheric Science, Florida State University, Tallahassee, FL, USA

Florida Climate Institute, Florida State University, Tallahassee, FL, USA

J. M. Collins, K. Walsh (eds.), *Hurricane Risk*, Hurricane Risk 1,
https://doi.org/10.1007/978-3-030-02402-4_3

3.1 Introduction

In the first two decades of the twenty-first century, a series of North Atlantic tropical cyclones (TCs) with large wind fields made landfall in the United States. These expansive storms – including Hurricanes Ivan (2004), Katrina (2005), Ike (2008), Irene (2011), Sandy (2012), and Irma (2017) – served as further evidence that damage potential is tied to much more than just the oft-reported maximum sustained wind intensity metric. Irene and Sandy, in particular, had top wind speeds that would not rank highly on the Saffir-Simpson Hurricane Wind Scale (SSHWS) just before they came ashore (Fig. 3.1), yet both storms caused considerable wind and surge damage, exceeding what is typically expected for storms of a similar intensity.

Certainly, intensity metrics are still quite useful, as there is clear indication that wind damage from TCs is connected to inner core wind speeds (e.g. Kantha 2006; Pielke and Landsea 1998; Murnane and Elsner 2012). Specifically, Murnane and Elsner (2012) indicate that losses and maximum sustained wind speeds are exponentially related, with an increase of loss at a rate of 5% per m s^{-1} of peak winds. However, beyond these high inner core wind speeds, a common meteorological feature that is relevant to the damage caused by some of these recent landfalling hurricanes is the overall size and structure of their wind field. For instance, a wide swath of tropical storm strength winds ($\geq$17 m s^{-1}) in larger TCs contributes to an increased volume of destruction and a more widespread wind threat to the population. Zhai and Jiang (2014) indicate that using a combination of storm size and maximum wind speed explains a larger portion of the variance in losses caused by a landfalling hurricane than using intensity (or size) alone. In an illuminating example, they suggest that economic losses from the landfall of Hurricane Sandy would have been approximately 20 times smaller if its size were comparable to an average sized TC, leaving its maximum sustained winds unchanged as observed.

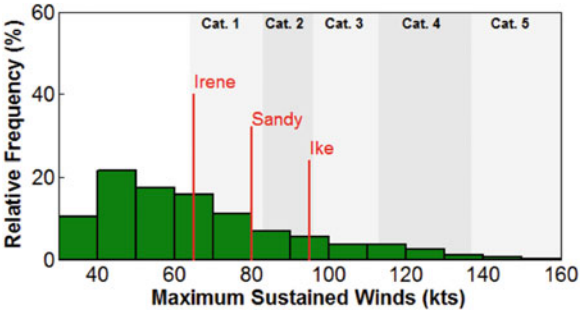

Fig. 3.1 Relative frequency distribution of six-hourly V_{max} measurements in Atlantic TCs between 1990 and 2011. This sample includes 5498 fixes from 291 storms. Vertical lines are shown to indicate V_{max} values for selected hurricanes just prior to a US landfall. The times of these V_{max} measurements are as follows: Ike 9/13/08 00Z; Irene 8/28/11 06Z; Sandy 10/29/12 18Z. The three storm points would fall in the top 45% of all TCs points in terms of V_{max} from 1990 through 2011. (Adapted from Kozar and Misra 2014)

Furthermore, storm surge from landfalling TCs continues to be a significant threat and has caused considerable damage historically (Pielke and Landsea 1998). Irish et al. (2008) found that there is a significant direct relationship between the size of a TC's wind field and the resulting peak surge, especially in regions with mildly sloping coastal bathymetry. Given that coastal developments continue to expand and become more densely populated (Crosset 2004), society is becoming more at risk to the wind and water from landfalling TCs. Given these increasing risks and the importance of storm size to the amount of lives and property exposed to the hazards associated with TCs, there is a rising interest in understanding and predicting the size and structure of TC wind fields (Cangialosi and Landsea 2016; Knaff et al. 2016).

In an effort to better evaluate the damage potential of TCs as a function of winds across the entirety of a TC, Powell and Reinhold (2007) introduced a novel, alternative metric called Integrated Kinetic Energy (IKE). This metric is proportional to a simple integration of one-half of the square of the 10-m wind field over a one-meter depth out to the radius of 34-knot winds:

$$\mathrm{IKE} = \int_v \frac{1}{2}\rho U^2 dV \tag{3.1}$$

IKE is tied to physical processes that cause damage, as it scales with wind stress on the ocean and the wind load forcing on structures (Powell and Reinhold 2007). Furthermore, given its integrated nature, IKE takes into account both inner core winds (i.e. TC intensity) and the size of hurricane wind fields, giving it potential advantages over more limiting intensity metrics which do not consider storm size at all. This is clearly demonstrated by hurricanes Irene, Ike, and Sandy, which each made landfall with IKE values that rank in the top 7.5% of historical values from 1990 to 2015, in contrast to their somewhat lower maximum sustained wind placement (Figs. 3.1 and 3.2).

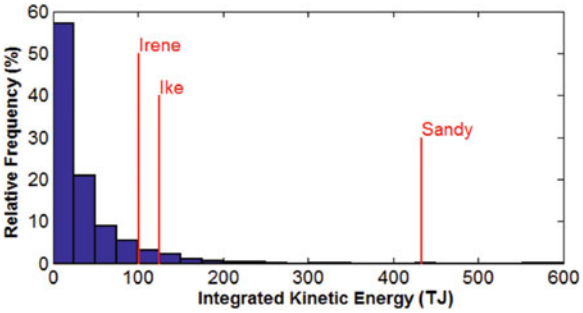

Fig. 3.2 Relative frequency distribution of six-hourly IKE measurements in Atlantic TCs between 1990 and 2011. This sample includes 5498 fixes from 291 storms. Vertical lines are shown to indicate IKE values for selected hurricanes just prior to a US landfall. The times of these IKE measurements are as follows: Ike 9/13/08 00Z; Irene 8/28/11 06Z; Sandy 10/29/12 18Z. The three storm points would fall in the top 7.5% of TCs in terms of IKE from 1990 through 2011. (Adapted from Kozar and Misra 2014)

The next section of this chapter will focus on the analysis of historical IKE values across the North Atlantic basin with a focus on how the metric can be measured or approximated, followed by a discussion on the climatology of IKE in North Atlantic tropical cyclones. Afterward, a series of sensitivity tests is presented to explore relationships between the environment, storm-scale features, and IKE, which might offer some guidance on how IKE could respond in a changing climate. Finally, an application will be presented in which IKE can be used to evaluate interannual TC activity (Sect. 3.4), with a discussion on how seasonal sums of IKE vary with changes in climate processes.

3.2 Analysis of IKE

3.2.1 Estimating Observed IKE

The biggest strength of the IKE metric is its consideration of the distribution and strength of surface winds across the entirety of a TC's wind field. However, by considering winds across such a large area, calculating IKE exactly in either a real-time or historical setting poses some potential challenges. Observations from aircraft reconnaissance serve as the most useful source of information when assessing storm size and structure. Other observational platforms such as buoys, ships, radar, and surface-based anemometers along the coast can also be of great use to measure the size and structure of TC wind fields, as demonstrated by the HRD real-time hurricane wind analysis system (H*Wind; Powell et al. 1998). When available, observationally-based gridded wind fields from analyses such as these are the preferred framework for calculating IKE directly (Powell and Reinhold 2007).

However, the critically important aircraft reconnaissance flights are not necessarily continuous in the Atlantic. For instance, Rappaport et al. (2009) reported that the coverage of these data is for only about 30% of all TC fixes in the North Atlantic. In other basins across the globe (e.g. West Pacific, Southern Hemisphere, and Indian Ocean), flight data may be absent altogether. The dearth of in situ observations in some locations has forced forecasters, analysts, and researchers alike to rely more heavily on wind field estimates from satellites (Knaff et al. 2016). These satellite-based winds may come from multiple sources, including microwave radiometers (Demuth et al. 2004, 2006), scatterometers (e.g. Atlas et al. 2011; Holmlund et al. 2001), and cloud drift winds (Velden et al. 2005). Ultimately, spaceborne retrievals are quite useful for filling gaps where surface data might not otherwise exist, but these techniques still have their own limitations. For instance, scatterometers often underestimate the inner core wind speeds within intense TCs (e.g. Brennan et al. 2009), and retrievals are susceptible to contamination from high rain rates throughout the storm (e.g. Weissman et al. 2012). As technology improves and new observation platforms become available in the coming years (e.g. GOES-16, CYGNSS, etc.), it is likely that measurements of hurricane wind structure will

improve both in quality and duration, allowing for better estimation of IKE (Morris and Ruf 2016).

In the meantime, given the inconsistent coverage and quality of hurricane wind measurements around the world, it may be difficult to compute IKE directly from observations in all cases. Other gridded datasets such as numerical reanalysis provide another option for estimating historical values of IKE across the globe in a more consistent framework. However, gridded wind reanalyses continue to show a persistent weak TC bias and often are unable to resolve smaller TCs (Manning and Hart 2007; Schenkel and Hart 2012; Buchanan et al. 2018), making them less than ideal for directly calculating the IKE of a TC's wind field in most cases.

Given the challenges of calculating IKE directly, Misra et al. (2013) offered an alternative method for approximating IKE through an empirical relationship between reported operational wind radii. Estimates of storm size are already provided by many of the TC warning centers (e.g. National Hurricane Center [NHC], Central Pacific Hurricane Center [CPHC], Joint Typhoon Warning Center [JTWC]) in their regular advisories. These operational values are often stored and/or reanalyzed after the season in research and operational datasets such as the Automated Tropical Cyclone Forecast System (ATCF) b-decks or the NHC's HURDAT2 database and the Extended Best Track (Demuth et al. 2006). Size is typically reported in datasets such as these by providing approximations of the maximum radial extent of 34-kt (tropical storm force), 50-kt (storm force by Beaufort wind scale; WMO 1970) and 64-kt (hurricane force) winds in cardinal geographic quadrants (northwest, southwest, southeast, and northeast) from available data platforms. The aforementioned data quality and coverage inconsistencies surely affect the accuracy of the operational radii metrics (e.g. Landsea and Franklin 2013). Furthermore, Vigh et al. (2012) specifically notes that some parameters such as the radius of maximum winds often do not match actual aircraft measurements particularly well in the early portions of the Extended Best Track data (i.e. pre-2001). Nonetheless, Knaff et al. (2016) indicate that the best track wind radii from the NHC provide useful estimates of TC wind radii for developing new techniques.

Table 3.1 details the algorithm to compute IKE from discretized wind radii data adapted from Misra et al. (2013). These formulas may be used in conjunction with the HURDAT2 and the Extended Best Track dataset to provide a continuous estimate of IKE for all storms in the Atlantic basin, going back almost three decades in a reasonably consistent framework. Such a dataset of IKE values, while inexact, would still be useful for analyzing the climatology of IKE in storms across the North Atlantic basin.

3.2.2 Climatology of IKE in the North Atlantic Basin

Applying the algorithm in Table 3.1 to the radii data in HURDAT2 and the Extended Best Track dataset yields a historical dataset containing IKE estimates for more than 5600 six-hourly fixes for nearly 300 storms between 1990 and 2011 in the North

Table 3.1 Algorithm to compute IKE from discretized wind radii data (e.g. Extended Best Track data Demuth et al. 2006) (From Misra et al. 2013)

Quadrant IKE contribution	Criteria	Mean wind (m s^{-1})	Area
$IKE_{18–26}$	R_{26} >0	20	1/4 π ($R_{18}{}^2$–$R_{26}{}^2$)
	No R_{26}, V_{MS}>26, R_{18}>R_{max}	20	1/4 π ($R_{18}{}^2$–(0.75R_{max}) ^{2})
	No R_{26}, V_{MS}<26, R_{18}>R_{max}	1/4 V_{MS} + 3/4 (18)	1/4 π ($R_{18}{}^2$–(0.75R_{max}) ^{2})
	No R_{26}, R_{max}=R_{18}	18	1/4 π ($R_{18}{}^2$–$(0.5R_{18})^2$)
$IKE_{26–33}$	R_{33}>0	27.75	1/4 π ($R_{26}{}^2$–$R_{33}{}^2$)
	no R_{33}, V_{MS}>33, R_{26}>R_{max}	27.75	1/4 π ($R_{26}{}^2$ −$(0.75R_{max})^2$)
	no R_{33}, V_{MS}<33, R_{26}>Rmax	.25 V_{MS}+.75 (26)	1/4 π ($R_{26}{}^2$–(0.75R_{max})^2)
	no R_{33}, R_{26}<=R_{max}	26	1/4 π [$R_{26}{}^2$–$(.5R_{26})^2$]
IKE_H	Max R_{33} Quadrant, R_{33}>R_{max}	.25V_{MS} +.75 (33)	1/4 π ($R_{33}{}^2$–(0.75R_{max})^2)
	Max R_{33} Quadrant, R_{33}= R_{max}	.25V_{MS} +.75 (33)	1/4 π ($R_{33}{}^2$–$(.75\ R_{33})^2$)
	R_{33}<R_{max}	.1V_{MS} + .9(33)	1/4 π ($R_{33}{}^2$–$(.75\ R_{33})^2$)
	Not max R_{33} Quadrant	.1V_{MS} + .9(33)	1/4 π ($R_{33}{}^2$–(0.75R_{max}) ^{2})
	R_{max} = R_{33}		

R_{18}, R_{26}, R_{33}, refer to radius of wind speeds of 18, 26, 33 ms^{-1}, R_{max} is radius of maximum winds and V_{MS} is speed of maximum sustained wind speed of the TC

Atlantic Basin. Only fixes for subtropical storms and TCs are used in this dataset, but certainly some of the included fixes will correspond to storms that are ongoing but have not completed extratropical transition. Across this wide sample of IKE fixes (of which the distribution is plotted in Fig. 3.2), the mean six-hourly IKE value is 35.4 TJs. The distribution is skewed towards lower values with more than 57% of the fixes containing less than 25 TJ of IKE. Consequently, the standard deviation of IKE values is relatively high (43.6 TJ), and there is a long tail of high IKE values in the record. Sandy in 2012 and Igor in 2010 are two recent members of this long tail, as both obtained more than ten times the mean IKE value by the end of their lifetime. Overall, the shape of the distribution for this large number of IKE samples resembles a log-normal distribution (Kozar and Misra 2014), which was also proposed as a good fit for the distribution of storm size as measured by the radius of vanishing wind (Dean et al. 2009).

Further dissection of the historical dataset reveals that over the course of a storm's lifetime, it will peak at approximately 50 TJ of IKE on average. More than a quarter of the 291 storms in the record never grow past 10 TJ of IKE at any one time, with only a fifth of the historical storms ever reaching 100 TJs during their lifetime.

The seasonal cycle of the IKE values in this record follows somewhat closely the seasonal cycle of TC frequencies in the North Atlantic, except it is skewed a little bit

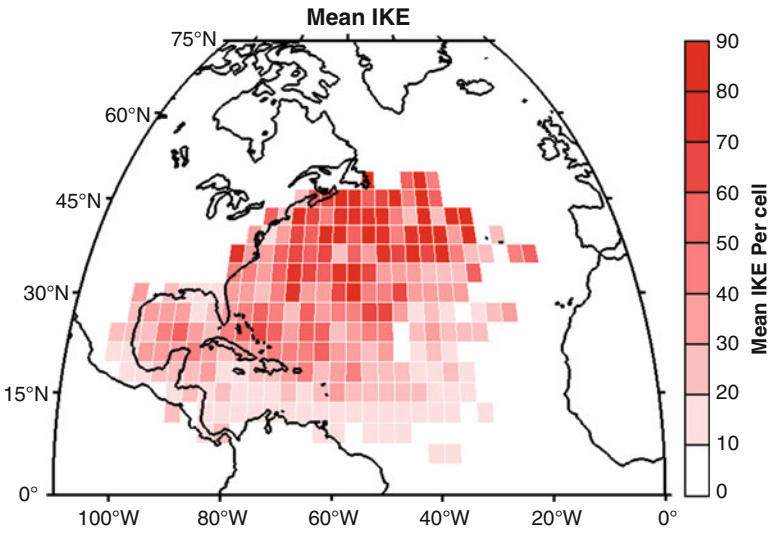

Fig. 3.3 Map showing historical mean IKE values for all fixes from 1990 to 2011 spatially across $3 \times 3°$ bins in the North Atlantic. The distribution of mean IKE suggests that storms have higher IKE on average in the northern most latitudes of the basin. Please note that the grid cells in the higher latitudes will be smaller in area than the grid cells over the deep tropics in this figure and the two that follow

more towards the end of the typical hurricane season. The mean monthly IKE value peaks in September at 44 TJ, or approximately 25% higher than the overall mean (not shown). Mean six-hourly IKE values are higher in October and November than they are in June, July, or August, indicating a preference for storms with higher IKE values later in the season.

Looking now at the spatial climatology of IKE across the Atlantic, it becomes evident that storms climatologically obtain higher IKE values as they move poleward in the northern part of the basin (Fig. 3.3). This is consistent with the higher IKE values found later in the season, as many TCs that form in October and November occur in the western half of the basin and follow a more meridional track toward the pole. Meanwhile, TCs over the main development region in the central Atlantic and Caribbean typically have less IKE, with a few other localized maxima appearing in the Gulf of Mexico and over the Bahamas. Focusing on only IKE values that exceed 100 TJ in the historical record, it becomes even more apparent that the western and northern parts of the basin are preferred regions for high IKE values (Fig. 3.4). Furthermore, storms tend to obtain their lifetime peak IKE value at the end of their tracks either in the northern part of the basin as they recurve or just before making landfall in the western edges of the basin (Fig. 3.5). This tendency for IKE to maximize in the northwest part of the basin does not necessarily overlap with where one might expect the most intense storms to be located, which would likely be further south.

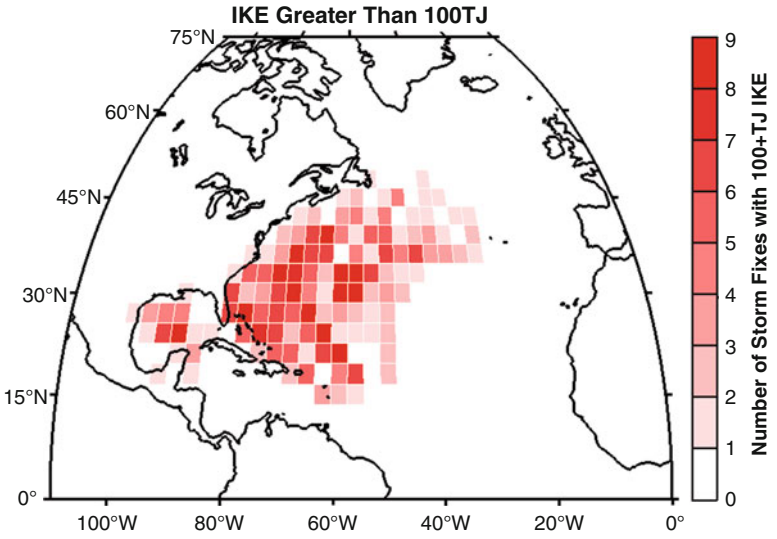

Fig. 3.4 Map showing where tropical cyclones between 1990 and 2011 had IKE exceeding 100TJ, gridded into $3 \times 3^{\circ}$ bins

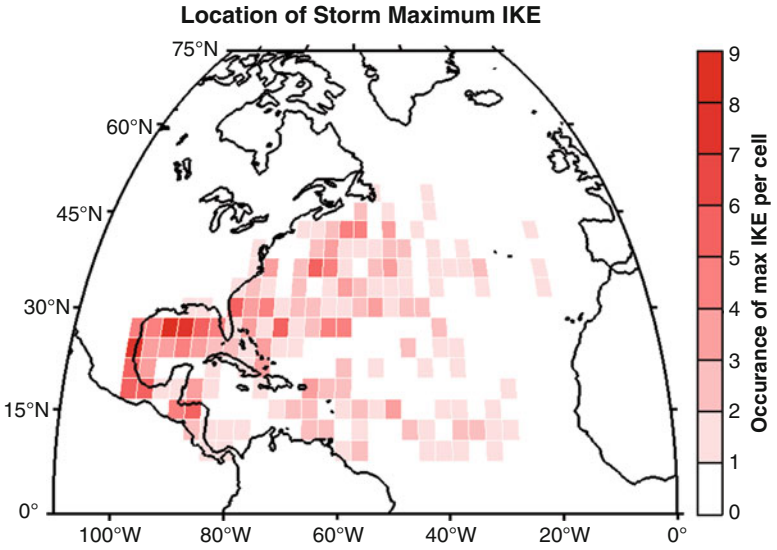

Fig. 3.5 Map showing where tropical cyclones reached their maximum lifetime IKE values from 1990 to 2011, gridded into $3 \times 3^{\circ}$ bins

Indeed, the northwestern part of the basin does not necessarily include the most favorable conditions for traditional TC development throughout most of the year. With the exception of areas along the Gulf Stream, sea surface temperatures (SSTs)

are often cooler in the northern part of the basin, and vertical wind shear also tends to be higher, suggesting that baroclinic effects or trough interactions in the mid-latitudes may be vital for creating and sustaining high IKE storms. All of this suggests that the factors that govern IKE variability are complex and likely regional, with the northern part of the basin likely impacted by more than just the processes that govern traditional intensification. Maclay et al. (2008) indicated that observed intensity and kinetic energy metrics from observations across the basin fit reasonably well to a power law function, with kinetic energy increasing by an order of $(V_{max})^{1.872}$. However, a scatter plot of intensity and IKE shows two different relationships for storms north or south of 30°N latitude (Fig. 3.6). In the southern part of the basin, IKE is tied to intensity, with the two quantities having a correlation of 0.65 (significant at the $p = 0.01$ level). In contrast, IKE and intensity are less correlated in the northern part of the basin, with the highest IKE values all occurring in an intensity sweet spot centered on the lowest Saffir-Simpson Scale category or two.

The evolution of kinetic energy and intensity has been explored at length previously. Musgrave et al. (2012) suggested that the lifecycle for a TC contains three stages—incipient, deepening, and mature—with intensification occurring in the first two phases and kinetic energy growth occurring throughout all phases. The incipient phase includes more gradual increases in kinetic energy and intensity, before intensity begins to increase more rapidly during the deepening phase. Maclay et al. (2008) found that intensifying storms over warm waters and with low shear typically saw less kinetic energy growth than would be expected by the aforementioned power law KE-V_{max} relationship, as these wind speed increases are more confined to the inner core. Putting this all together helps to explain why mean IKE values in the southern half of the basin tend to be more moderate—increasing a little bit more as storms reach the western Caribbean and Gulf of Mexico—as traditional intensification mechanisms typically only increase IKE so far.

However, as Musgrave et al. (2012) points out, kinetic energy continues to increase during the mature phase of a TC, long after the storm reaches its maximum lifetime intensity. In fact, many storms gain IKE quite rapidly as they turn poleward, which likely can be attributed to external forcing from baroclinic influences, trough interactions, and extratropical transitions, which can help to promote increased angular momentum, wind field expansion, and some inner core intensification simultaneously (e.g. Maclay et al. 2008). An IKE-V_{max} diagram of Hurricane Igor in 2010 (Fig. 3.7) serves as a good example that fits closely to the idealized lifecycle for a TC as detailed by Musgrave et al. (2013). IKE increased throughout much of the Igor's lifecycle with the most drastic increase in IKE occurring as Igor interacted with a trough in the mid-latitudes prior to becoming extratropical, causing its lifetime maximum IKE value to be at the end of its life as a tropical cyclone.

Of course, there are many additional processes that can interrupt the idealized evolution of IKE during a TC's lifecycle (and thus the climatological preferences of IKE in the basin) that have not been discussed above. Land interactions are one obvious and noteworthy event that often results in large changes across a TC's structure (e.g. potentially increasing the radius of maximum winds and the general decay of wind speeds over land), which of course will impact IKE. In addition, Sitkowski et al. (2011) found that concentric eyewall replacement cycles also greatly affect the IKE in a

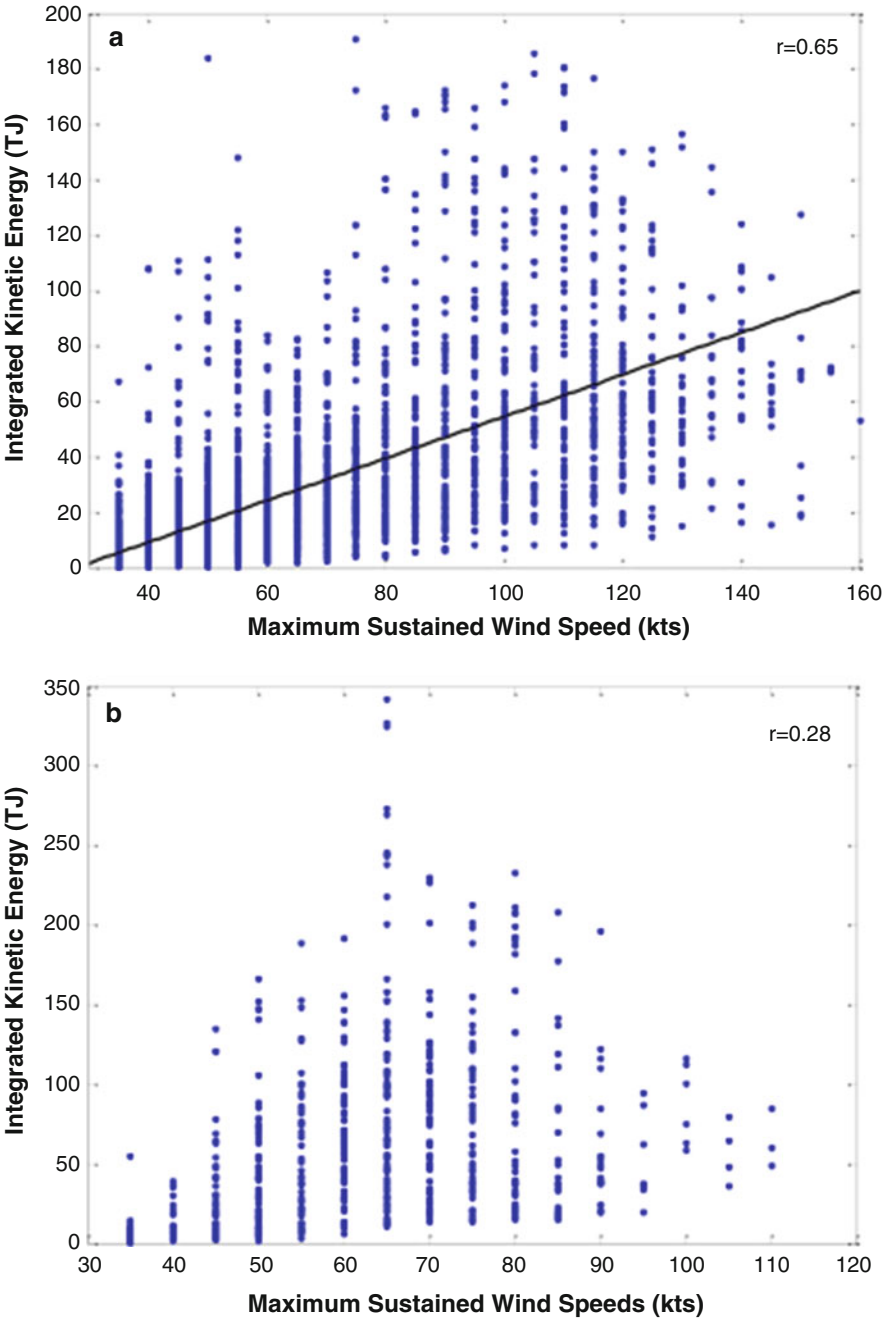

Fig. 3.6 (**a**) Plot of integrated kinetic energy (TJ) versus maximum intensity (kts) for 3896 Atlantic TCs located south of 30°N latitude between 1990 and 2011 (blue dots). The black line represents a linear regression fit for the data. Considering the large sample of storm fixes, the linear correlation is

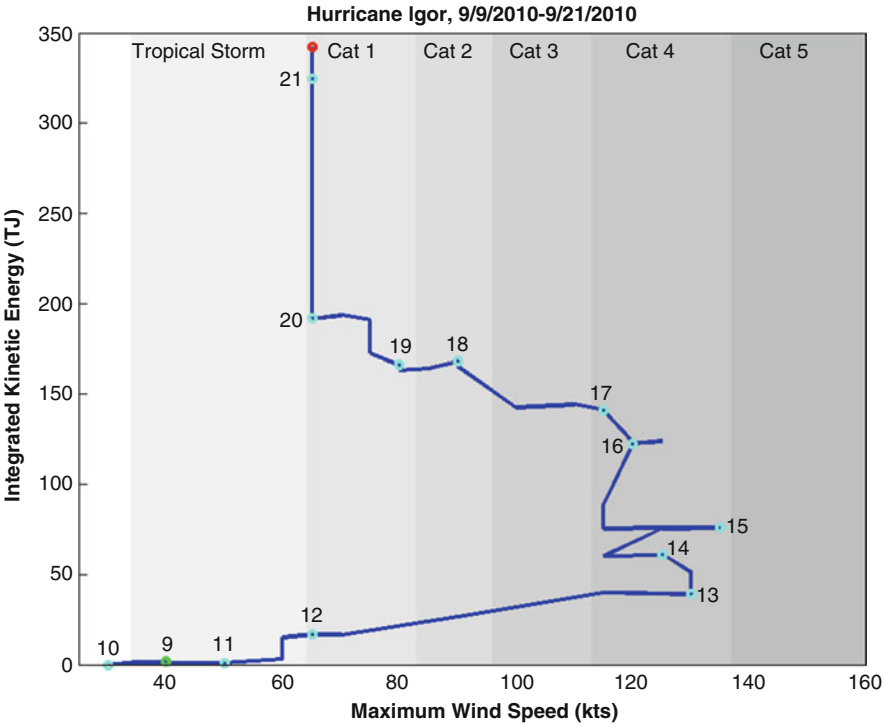

Fig. 3.7 Evolution of integrated kinetic energy (TJ) versus maximum intensity (kts) throughout the lifetime of Hurricane Igor in September of 2010 following Musgrave et al. (2012). The first point on the plot temporally (green circle) occurred on September 9, 2010, shortly after Igor obtained Tropical Storm intensity for the first time. Each of the subsequent cyan circles signals a 00Z storm fix, indicating the passage of a day's time, with the final fix occurring on September 21, 2010 (red circle) when Igor completed its extratropical transition over the North Atlantic

TC's wind field, with an average increase of 28% in a sample of 24 events. Musgrave et al. (2012) visualized these eyewall replacement cycles in the IKE-V_{max} diagram as a brief excursion to lower intensities with continued IKE growth.

3.3 Statistical-Dynamical Sensitivity Tests for Studying IKE Variability

As was summarized in the previous section, IKE has some notable climatological preferences, some strong ties to environmental conditions, and the tendency to increase throughout a TC's lifetime. All of these factors can be leveraged to model

Fig. 3.6 (continued) easily significant at the $p = 0.01$ level. (**b**) Plot of integrated kinetic energy (TJ) versus maximum intensity (kts) for 735 Atlantic TCs located north of 35°N latitude between 1990 and 2011. The correlation between VMAX and IKE in this figure is $r = 0.28$

IKE variability using a statistical-dynamical model of atmospheric and oceanic parameters. Kozar and Misra (2014) and Kozar et al. (2016) offered a proof of concept that IKE can be modeled skillfully relative to persistence and climatology. These models might be used not only for future forecasting applications (with dynamically forecasted predictors), but can also be quite useful for further analyzing the relationships between IKE and the environment, as is done here using a set of sensitivity tests.

For these sensitivity tests, we utilize the system of artificial neural networks presented by Kozar et al. (2016). This statistical-dynamical system, named the Statistical Prediction of IKE Version 2 (SPIKE2), was designed to analyze and hindcast IKE variability in North Atlantic TCs. It builds upon the linear regression techniques used in the first version of SPIKE (Kozar and Misra 2014), by incorporating the intrinsic nonlinear map of weights within the neural networks, which allowed SPIKE2 to anticipate the nonlinearities within the environment-TC system. For example, in traditional TC development, wind shear is typically negatively correlated with inner core intensity and IKE; however, in the mid-latitudes, an increase in shear (to an extent) might benefit outer wind field expansion as extratropical transition often causes wind fields to increase in size (e.g. Evans and Hart 2008). In a linear regression approach, it would be impossible to tease out these complex signals, but the neural networks used for SPIKE2 possess the flexibility to potentially anticipate these signals within the training dataset.

To best estimate how the SPIKE2 neural networks would perform in a forecast realm, Kozar et al. (2016) focused on neural networks that were calibrated and evaluated using reanalysis and hindcast data from the second generation GEFS reforecast project (Hamill et al. 2013). Despite the predictors containing some degree of modeling uncertainty and forecast error, SPIKE2 performed well and was skillful relative to both climatology and persistence out to 72 h. In fact, for a 24-h hindcast, SPIKE2 explained more than 80% of the variance in the IKE record. Despite the impressive hindcast results, this section will move the neural networks back into the perfect prognostic space using historical predictors. The historical predictors in the perfect prognostic space do not contain forecast errors and are better suited for an exercise seeking to best understand how the environment modulates IKE in observed North Atlantic TCs.

In this perfect prognostic setup, SPIKE2 is calibrated and evaluated with eighteen predictors (Table 3.2) to estimate 36-h changes of IKE. The input predictors include metrics relevant to large scale atmospheric/oceanic dynamics and thermodynamics (e.g. deep layer wind shear, upper atmospheric temperatures, relative humidity, sea surface temperatures, and upper level divergence), storm specific parameters (minimum central pressure, maximum wind speed, center position, time since genesis, etc.), and a series of persistence parameters (past 12-h change of intensity and 36-h IKE persistence). Ultimately, these parameters were chosen from a larger pool of candidate predictors based on their physical relationship to storm size and strength, and their significance for statistically modeling IKE. The neural networks were

Table 3.2 List of eighteen predictors used to calibrate the perfect prognostic version of the SPIKE2 neural networks that is used in the sensitivity tests

Variable	Definition	Units
PIKE	36 h persistence of IKE	TJ
dIKE12	Previous 12 h change of IKE	TJ
VMAX	Maximum sustained wind speed	kts
VMPI	Difference between maximum potential intensity and VMAX	kts
LAT	Latitude of storm's center	°N
LON	Longitude of storm's center	−°W
MSLP	Minimum sea level pressure	hPa
PENV	Average surface pressure *(averaged from r = 200–800 km)*	hPa
VORT	850 hPa vorticity *(r = 0–1000 km)*	10^{-7} s^{-1}
D200	200 hPa divergence *(r = 0–1000 km)*	10^{-7} s^{-1}
SHRD	850–200 hPa shear magnitude *(r = 200–800 km)*	kts
SHTD	850–200 hPa shear direction *(r = 200–800 km)*	°
RHLO	850–700 hPa relative humidity *(r = 200–800 km)*	%
RHMD	700–500 hPa relative humidity *(r = 200–800 km)*	%
T150	150 hPa temperatures *(r = 200–800 km)*	°C
SST	Sea surface temperatures	°C
SDAY	Time after tropical storm genesis	days
PDAY	Time from peak of season (Sept. 10)	days

constructed with an optimal number of nodes for these predictors to minimize the chances of overfitting. Kozar et al. (2016) offers a more complete discussion on the construction of the neural network and the selection of the predictors in greater detail. For brevity, each of these parameters will be referred to by its abbreviation in Table 3.2 throughout the remainder of this section.

Most of the eighteen parameters are extracted directly from the Statistical Hurricane Intensity Prediction Scheme (SHIPS)'s developmental dataset (DeMaria and Kaplan 1999), while others are taken from the NOAA Optimum Interpolation SST ("OI SST"; Reynolds et al. 2007) dataset and the NHC best track dataset (Jarvinen and Neumann 1979, Jarvinen et al. 1984). In the end, all predictors are normalized by the mean and standard deviation of the observed sample, which is comprised of more than 15 years of Atlantic TC data. Of course, the corresponding IKE targets used in calibration of the neural networks are taken from the wind radii-based historical record that has been described at length in the previous sections. Overall, the neural networks are trained on these 18 parameters for more than 3000 six-hourly storm fixes between 1995 and 2011.

The resulting statistical fit between SPIKE2's estimates of IKE and the historical record of IKE is a correlation greater than 0.90. The observed distribution of 36-h IKE tendency is also modeled reasonably well when given historical parameters (Fig. 3.8), albeit the modeled IKE tendency values are skewed more towards small

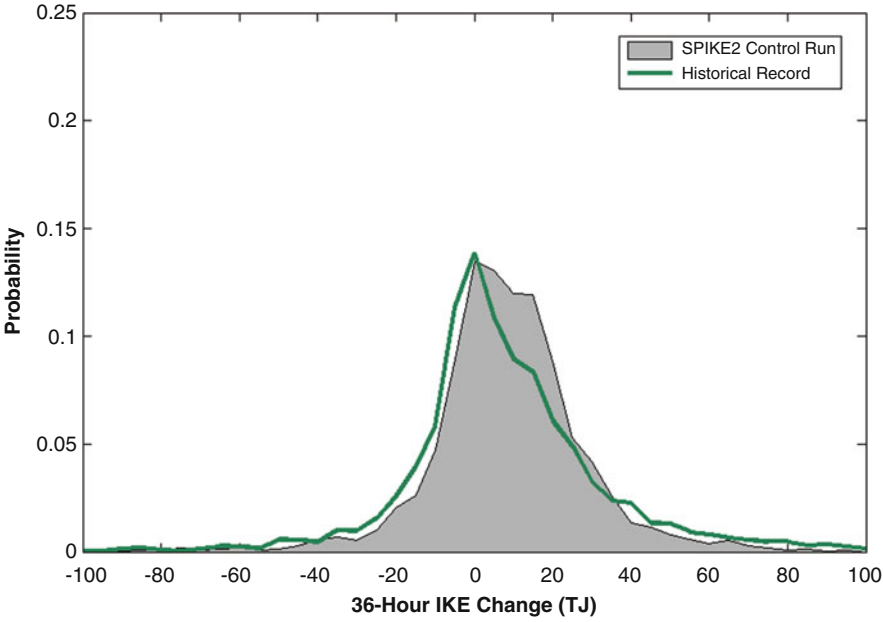

Fig. 3.8 Probability distribution of 36-h IKE change from the control run of the SPIKE2 neural network system and from the historical record. Approximately 3000 storm fixes from 1995 to 2011 are included in this distribution

increases of IKE than is observed. Given SPIKE2's ability to recreate the historical record of IKE, we are interested in learning how sensitive the modeled IKE estimates are to each predictor. As such, we will use a run of SPIKE2 with the unaltered historical parameters as the control run, and then each parameter will be perturbed one at a time by $\pm 1\sigma$ and $\pm 2\sigma$ for all of the 3000 fixes in the training dataset to examine how the nonlinear statistical model responds to perturbations in the environment. The distributions of IKE tendency as predicted by SPIKE2 in each perturbation run will be plotted against the control to best approximate how changes in the storm or the environment are likely to influence IKE tendency in an Atlantic TC (Fig. 3.9). Furthermore, the median of the distributions from each perturbation run is compared to the control run to see whether or not the distributions of IKE tendency systematically shift towards more negative or positive values (Table 3.3). The results of this sensitivity test are discussed at length by Kozar (2015), with the most significant results discussed in the remainder of this section.

Overall, the modeled distribution of IKE is most sensitive to the persistence and intensity parameters, with a few dynamical, thermodynamical, and positional parameters also having a significant impact on IKE variability. The significance of the persistence parameter is not entirely surprising. The positive shift in the distribution for the negative IKE perturbation test indicates that smaller developing TCs with less

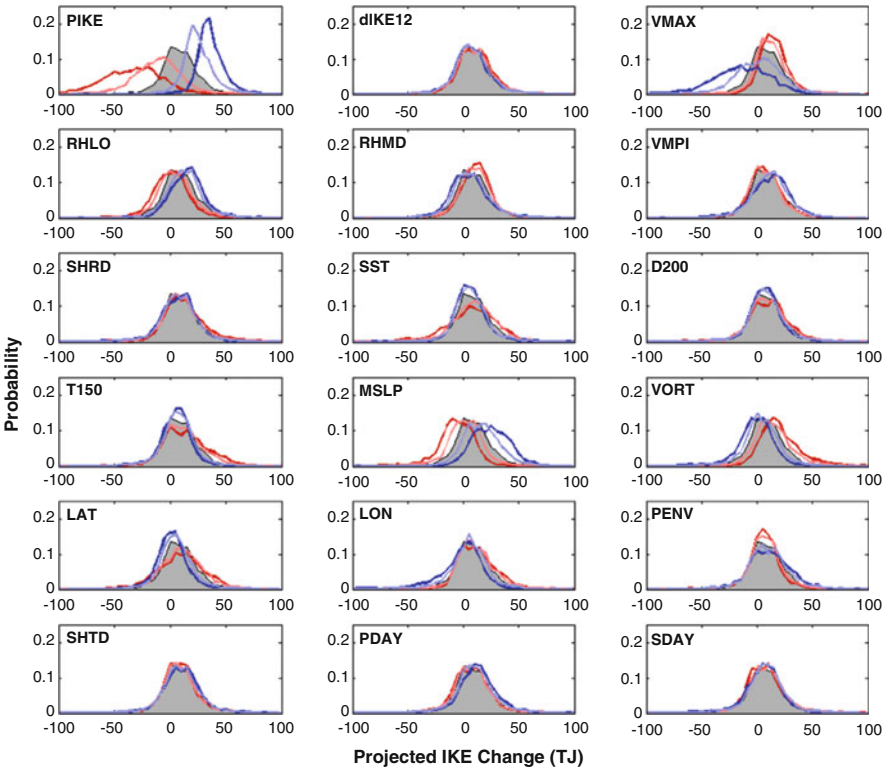

Fig. 3.9 The results of the sensitivity exercise are presented by showing how variations of each input parameter affect the probability distribution of a 36-h deterministic projection of IKE change from SPIKE2 for nearly 3000 TC fixes in the North Atlantic basin. The probability distribution for the control run is shown in each panel with a grey shaded polygon. The red curves show the distribution of projected IKE change from SPIKE2 when a single predictor is increased by one standard deviation (light red curve) or two standard deviations (dark red curve) for all historical TC fixes. The blue curves show the distribution of projected IKE change from SPIKE2 when each observed predictor is decreased by one standard deviation (light blue curve) or two standard deviations (dark blue curve) for all historical TC fixes

IKE are more likely to gain IKE, as long as other conditions are not too prohibitive, which is consistent with the theory that TCs gain IKE for most of their lifetime over the open ocean, even as intensity fluctuates, such that they obtain their maximum value of IKE prior to landfall or the completion of ET (Musgrave et al. 2012). In addition, this negative relationship between PIKE and IKE tendency is influenced by the fact that a storm with higher values of IKE obviously has more IKE to lose than does a smaller storm. Therefore, a storm with 100 TJs could theoretically lose or gain a large amount of IKE, causing the distribution of modeled IKE tendency to become broader for the positive PIKE perturbations.

Both intensity-related metrics – maximum sustained winds and minimum central pressure – have significant relationships with the modeled IKE tendency values. As

Table 3.3 Percent changes for median SPIKE2 projections of IKE tendency in each perturbation run relative to a control simulation

		Perturbations to Variables			
		−2σ	**−1σ**	**+1σ**	**+2σ**
Perturbed Input Parameter	**PIKE**	*268%*	*150%*	*−177%*	*−406%*
	dIKE12	*−13%*	*−8%*	11%	*25%*
	VMAX	*−215%*	*−61%*	*34%*	*59%*
	RHLO	*75%*	*45%*	*−39%*	*−71%*
	RHMD	*−37%*	*−20%*	*21%*	*32%*
	VMPI	*43%*	*36%*	*−17%*	−11%
	SHRD	*−2%*	*−3%*	*11%*	*31%*
	SST	*−21%*	*−16%*	*18%*	1%
	D200	*−6%*	*−4%*	10%	*26%*
	T150	*−23%*	*−9%*	*19%*	*46%*
	MSLP	*157%*	*79%*	*−62%*	*−133%*
	VORT	*−86%*	*−42%*	*49%*	*97%*
	LAT	*−62%*	*−33%*	*23%*	*12%*
	LON	*−69%*	*−25%*	*20%*	*28%*
	PENV	*23%*	*14%*	*−7%*	*−17%*
	SHTD	*24%*	*12%*	*−5%*	0%
	PDAY	*43%*	*17%*	*−4%*	*−9%*
	SDAY	*−16%*	0%	*−1%*	*−19%*

As discussed in Sect. 3.3, each perturbation run adjusts exactly one variable (leftmost column) up or down by either one or two standard deviations (topmost row). The resulting changes of IKE were tested for significance with a two-sample bootstrapping exercise. Those that are deemed significant at the two-sided 95% level are displayed in a italic font

intensity increases, IKE growth tends to be more prevalent, causing the distributions in Fig. 3.9 to shift to the right as VMAX is perturbed upward and MSLP downward. This result is not surprising, considering that Musgrave et al. (2012) showed the greatest gains in IKE to occur during the deepening and mature phases of a TCs life cycle. Despite their similarities, MSLP and VMAX interestingly affect the distribution of modeled IKE tendency values in vastly different manners. For instance, the negative VMAX perturbation runs have a broader distribution than the control run and any other VMAX or MSLP perturbation run. Therefore, a low intensity in terms of VMAX at the valid forecast time does not prevent SPIKE2 from projecting IKE to increase if other environmental parameters are favorable. In contrast, the distribution for the positive MSLP perturbation runs is shaped very similarly to the control run, albeit shifted to the left. This makes it less likely for TCs to gain an appreciable amount of IKE when its MSLP is high, as storms with higher central pressures are typically in their incipient phases (and not gaining IKE rapidly yet) or are approaching the end of their lifetime following decay in prohibitive environments (e.g. high shear or movement over land).

The differences between the distribution of the runs with negative VMAX and the distribution with positive MSLP perturbations arise because VMAX does not have a truly linear relationship with MSLP, with many operationally used pressure-wind relationships taking storm size and other environmental parameters into account (e.g. Knaff and Zehr 2007). For example, in the historical record, there are plenty of storms that have anomalously low minimum pressure levels, despite modest maximum wind speeds, especially in the mid-latitudes (e.g. Hurricane Sandy). Likewise, there are plenty of TCs that have modest values of VMAX (~50 to 70 kts) and anomalously high values of IKE (>100 TJ). As a result, it is not a surprise that the negative VMAX perturbation runs have a broader distribution to capture the possibility for high and low IKE storms depending on the other environmental and positional parameters.

On the subject of positional parameters, SPIKE2 also suggests that increasing latitude will result in IKE growth more often than not. The positive LAT perturbation runs have distributions that are skewed to the right when compared to the control run (Fig. 3.9). As a result, the median of the distribution for the $+1\sigma$ and $+2\sigma$ LAT perturbation tests is significantly greater than that of the control run at the 99% confidence level based on simple two-sample bootstrapping tests (Table 3.3). Interestingly, the distribution is not shifted quite as far away from the control run when compared with the MSLP, VMAX, and PIKE perturbation runs. This is not terribly surprising, considering that geographical positions are often overruled by the actual environmental conditions near the storm. As a result, the distribution of the positive LAT perturbation tests is somewhat broader than in the control run. This ultimately allows for a storm to have decreasing IKE when entering higher latitudes if the storm is not likely to undergo expansion from extratropical transition or trough interactions. In that regard, if a TC is over the high latitudes (LAT $= +1\sigma$), with cold oceans (SSTs $= -2\sigma$), with moderately low intensity (MSLP $= +1\sigma$; VMAX $= -1\sigma$), and its IKE has already begun to fall (dIKE $= -2\sigma$), SPIKE2 will project IKE to continue falling.

Dynamical predictors such as low-level vorticity also show some significant sensitivity to IKE variability (Table 3.3). Indeed, VORT has a strong positive relationship with modeled IKE tendency. Positive perturbations of VORT shift the distribution towards positive SPIKE2 projections, and the negative VORT perturbation runs result in a shift towards more negative IKE changes (Fig. 3.9). Overall, storm growth is projected to occur more frequently when VORT increases, and storm decay becomes more likely when a storm has either a small or weak vorticity signature, which is not surprising given that a stronger and larger circulation with high vorticity is indicative of high relative angular momentum and a strong cyclonic wind field.

Additionally, T150 also shows a significant relationship with the modeled IKE tendency distribution. The metric was used by Maclay et al. (2008) to examine kinetic energy variability, with the upper tropospheric temperatures standing in as a proxy for the tropopause height. Higher T150 values are indicative of a lower

tropopause, which is a characteristic of the higher latitudes. Given the tendency for the largest IKE changes to occur in the mid-latitudes (large gains from trough interactions, and large drops from storm decay over prohibitively cold waters), the negative T150 perturbations produce a narrower distribution, while the positive perturbations produce a wider distribution. The increase in moderate to large IKE gains in the positive T150 runs are consistent with the observed rapid growth in storms like Sandy and Igor.

On the other hand, some other predictors well known to influence TC development like SHRD and SST do not cause a systematic shift in the distribution of IKE tendency. This is likely due to the complexity of the nonlinear signals between these predictors and IKE. Through further testing it becomes clear that many of these predictors affect IKE variability in different environmental regimes. For instance, an extra perturbation test over the lower latitudes with negatively perturbed LAT and negatively perturbed T150 shows that IKE has a tendency to grow with increasing SST and decreasing SHRD, which is not true in higher latitudes where non-tropical mechanisms such as trough interactions and baroclinic forcing can allow storms to grow in size while possibly also increasing intensity briefly as storms begin to transition (e.g. Maclay et al. 2008).

Ultimately, the results presented from these sensitivity tests offer some clues on how the IKE of Atlantic TCs may respond to our changing climate. Some recent literature has suggested that stronger storms are migrating northward (e.g. Kossin et al. 2014; Baldini et al. 2016) as warm sea surface temperatures expand poleward. The sensitivity tests indicate that IKE growth is promoted when storms are more intense and in regions of higher latitude. As such, one could hypothesize that, all else being equal, a poleward shift in TC activity could promote greater increases in IKE on a per storm basis, as storms approach the Mid-Atlantic United States and interact with mid-latitude features. However, when focusing on just the North Atlantic, this poleward trend might be less significant and might even be negative in the basin (Moon et al. 2015; Kossin et al. 2016).

Other studies have also indicated that the global tropics are expanding (Lucas et al. 2014) and that baroclinicity could become weaker in the mid-latitudes, which could affect the extratropical transition process (Ito et al. 2016). All of these factors, along with long-term variability in cyclogenesis and steering currents, could have ramifications for where TCs are most likely to gain IKE. Given all of the complexities within the dynamics and thermodynamics of a changing climate, more work is clearly needed to evaluate whether or not higher IKE storms will become proportionally more common in the future, and/or whether or not the regions for IKE gain will shift across the basin at all.

3.4 Lower Frequency IKE Variability and Seasonal Applications of IKE

The six-hourly historical IKE record in the Atlantic can also be used to investigate whether or not any longer-term trends exist for IKE in the Atlantic basin. Powell and Kozar (2015) presented some initial findings that focused on interannual IKE variability. There is some slight evidence of increased IKE values for storms in the North Atlantic basin over a 25-year sample from 1990 to 2014 (Powell and Kozar 2015). Linear trend lines for the frequency of storms that exceed 25 TJs and 50 TJs are both positive during this timeframe, but they were not significant by any measure. In fact, much of this positive trend can be attributed to the lower number of TCs in the early 1990s, relative to the high annual counts seen afterwards. The peak instantaneous IKE value observed in any storm for a given year, which is less dependent on TC frequencies, also contains a positive trend (Powell and Kozar 2015). However, it is important to note that this sample is relatively short for investigating variability on interannual and longer scales, allowing for anomalous years (2005) and anomalously high-IKE storms (e.g. Igor, Sandy) to dominate the longer-term signal. As such, further work and a longer historical record are both clearly needed to better understand longer-term variability of IKE in Atlantic. tropical cyclones.

The record of IKE values can also be extended to monitor seasonal TC activity by aggregating IKE values across the lifetime of all TCs in a given year. To this end, Misra et al. (2013) proposed the Track Integrated Kinetic Energy (TIKE), the sum of IKE over the TC lifetime, which has some similarity to Accumulated Cyclone Energy (ACE; Bell et al. 2000) and Power Dissipation Index (PDI; Emanuel 2005, 2007). However, these latter indices are critically dependent on the intensity, with ACE and PDI proportional to the second and third power of the maximum sustained wind speed of a TC, and ignore the size aspect of the TC. In contrast, TIKE is comprehensive, in that it integrates the size, the wind speed, and the life span of the TC. Misra et al. (2013) computed TIKE for each named TC in the North Atlantic between 1990 and 2011 by summing the IKE values every 6 h over the lifetime of the TC.

Analysis of average monthly TIKE values reveals a peak in September (Fig. 3.10) coinciding with the corresponding peak in larger and longer-living TCs in the same month (Misra et al. 2013). Meanwhile, annual TIKE values exhibit significant interannual variations that are comparable to variations in other metrics that measure seasonal Atlantic TC activity (Fig. 3.11). The correlation over the North Atlantic between TIKE and ACE is 0.86, between TIKE and number of storms is 0.61, and between ACE and number of storms is 0.78. There are some notable differences between TIKE and the other metrics, however. Yu et al. (2009) and later Yu and Chiu (2012) noted that the differences between seasonal metrics that incorporate storm size and those that are intensity-based will grow exponentially as storm intensities increase. As such, comparisons between TIKE and ACE, as well as annual TC counts, are quite illuminating (Fig. 3.11). For example, the 2005 season,

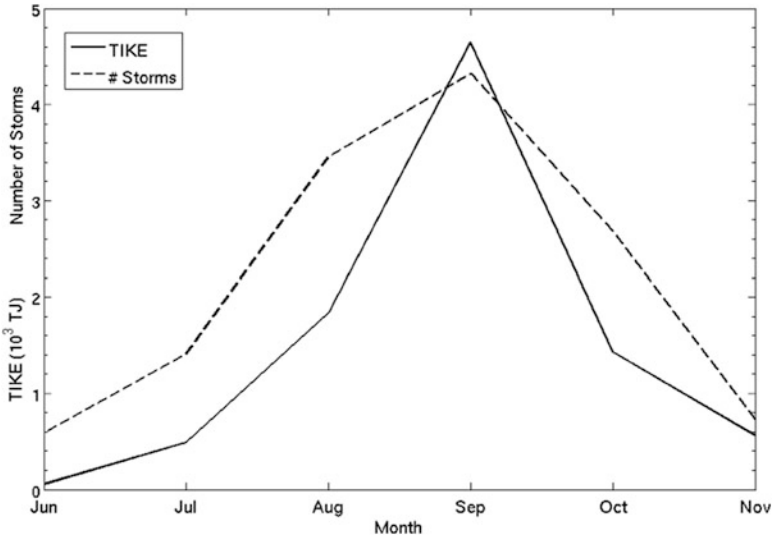

Fig. 3.10 Monthly climatology of TIKE and the number of tropical storms in the North Atlantic basin between 1990 and 2011. (From Misra et al. 2013)

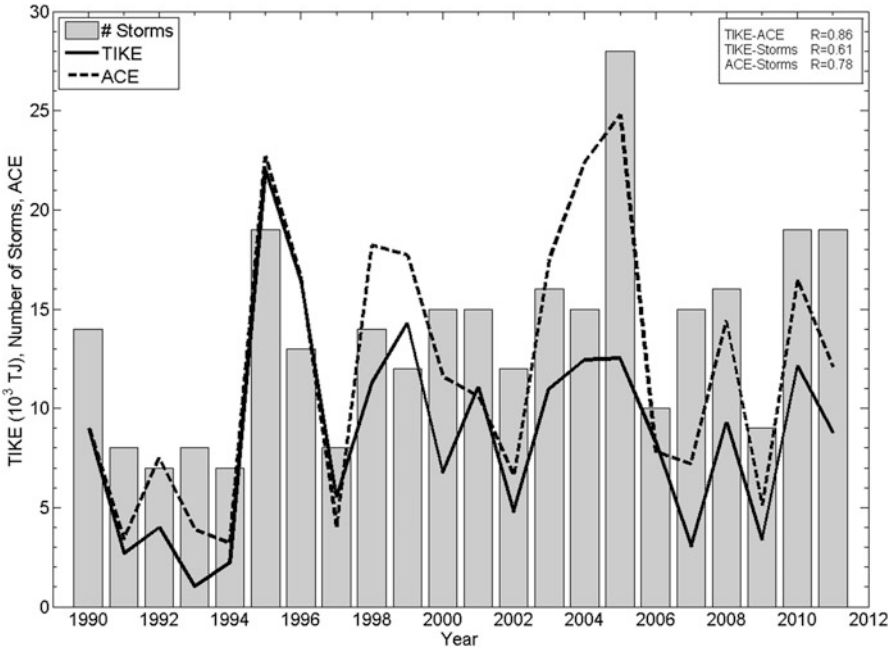

Fig. 3.11 Time series of TIKE, ACE and number of tropical storms in the North Atlantic basin from 1990 to 2011. (Adapted from Misra et al. 2013)

with its 28 named Atlantic TCs, appeared as a highly anomalous year in terms of ACE and the number of TCs in a season. However, TIKE proved to be far less anomalous in 2005. With the exception of a few notable storms such as Katrina, this comparison reveals that 2005 was not characterized by as many large-sized and long-lived TCs as other active seasons, such as 1995. Overall, the most anomalously high TIKE years were 1995 followed by 1996, 1999, and 2012, with 1993 and 2013 being the two least active years since 1990 as measured by TIKE.

Misra et al. (2013) also examined interannual variations of TIKE with global SST variations. Like most other indices of Atlantic TC activity (e.g. ACE), TIKE exhibits a robust relationship with SST variations in the equatorial Pacific associated with the El Niño Southern Oscillation (ENSO). Figure 3.12 suggests that a warm (cold) ENSO phase is associated with anomalously small (large) Atlantic TIKE. This is consistent with earlier studies which indicated that cold ENSO events are associated with not only increased TC activity as a whole, but also more recurving and landfalling TCs in the Atlantic (Bove et al. 1998; Kossin et al. 2010; Colbert and Soden 2012). In other words, cold ENSO events are associated with more TCs in the western tropical Atlantic and northern (extra-tropical) Atlantic, such that the existence of longer-lived and higher IKE storms is promoted, leading to a higher accumulation of TIKE throughout the course of a La Niña hurricane season.

Similarly, Misra et al. (2013) also investigated ties between interannual variations of TIKE and Atlantic Warm Pool (AWP) variability. The AWP is defined as the area enclosed by the 28.5 °C isotherm in the tropical-subtropical Atlantic Ocean and is a robust seasonal phenomenon that coincides with the Atlantic hurricane season (Wang and Enfield 2001). Ultimately, a positive correlation of 0.43 exists between TIKE of Atlantic TCs and the area covered by the AWP from August through October. In other words, large AWP seasons are associated with increased likelihood of larger values of TIKE and small AWP seasons are associated with smaller annual accumulations of TIKE.

Physically, this positive relationship between the size of the AWP and TIKE is consistent with the findings of earlier research. For instance, the AWP's interannual variability corresponds well with variations of the North Atlantic Subtropical High (NASH; Wang and Enfield 2001; Wang et al. 2006), which has implications for TC behavior in the entire basin. More specifically, a large (small) seasonal mean AWP is associated with a weakened (strengthened) NASH and increased (decreased) atmospheric convection and cloud cover over the AWP region. Furthermore, large seasonal AWPs correspond to weaker tropospheric vertical wind shear and a deep warm upper ocean, thus making the large-scale environment conducive for an active Atlantic TC season, with the opposite being true for small AWP seasons. Wang et al. (2011) also show that the AWP has a significant bearing on the steering flow of Atlantic TCs through its connections with the NASH, resulting in the likelihood of fewer United States landfalling TCs along the eastern seaboard during large AWP years. Putting all of this together, during large AWP years, the overall frequency of TC events is increased and storms tend to have longer life spans with larger radial

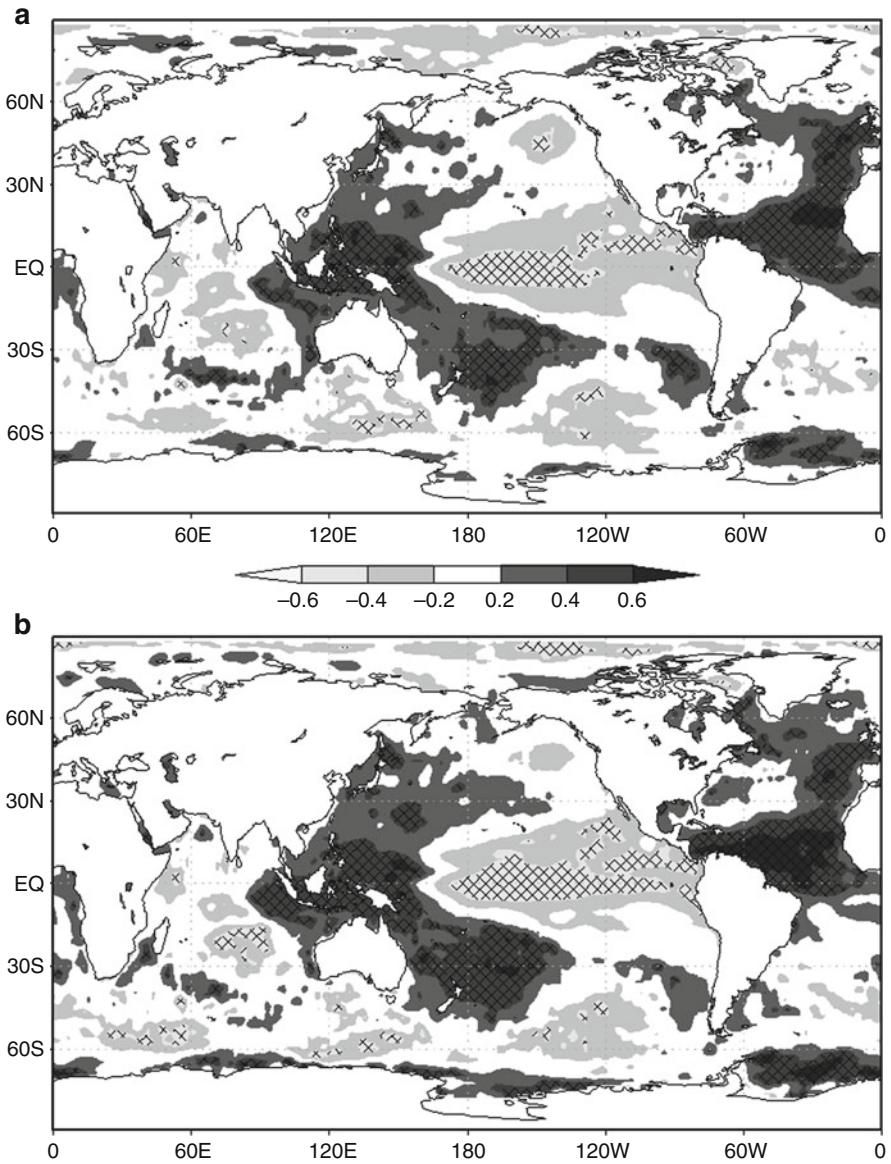

Fig. 3.12 Correlation of (**a**) TIKE and (**b**) ACE in the North Atlantic basin with contemporaneous seasonal mean SST anomalies from OISSTv2. Hashed regions show significance at the 95% confidence interval according to Student's t-test. (From Misra et al. 2013)

extents as they form further east and recurve away from the United States more frequently into an area that climatologically promotes higher IKE values. All of this ultimately ties back to an unsurprising positive relationship between interannual variations of TIKE and the AWP.

3.5 Summary and Conclusions

This chapter provides a review of IKE-related studies. The majority of these studies are confined to the North Atlantic basin, where aircraft observations are most prevalent and IKE can be consistently estimated from the historical record extending back to the 1990s. The other tropical basins are less data rich with fewer observations and more limited historical datasets. With the help of remotely sensed wind data the gaps in many of the world's oceans are being filled to some extent, and in a few years, it appears that IKE could be studied more extensively in all tropical basins.

IKE is demonstrably a very useful metric to characterize TCs. Its emphasis on size and wind structure around the azimuth of the TC provides a realistic estimate of the potential damage that TCs can cause upon landfall. IKE scales very well with wind stress over ocean and wind load forcing on structures that in turn relate to storm surge and wind damage respectively. Therefore, pursuing IKE as a complementary metric to existing practices to monitor and forecast TCs would be prudent, especially in efforts to guide in mitigating and avoiding risks from landfalling TCs.

IKE is intrinsically related to intensity metrics in a TC. The incipient, development, mature, and decay stages of a TC characterized in terms of its intensity metrics have distinct IKE tendency features as well. Although IKE typically increases through a storm's lifetime from traditional TC development mechanisms, the most rapid increase in IKE is often seen later in a storm's lifecycle as storms undergo expansion of their outer wind fields around the time of their extratropical transition. Modeling IKE and a series of environmental parameters offers some evidence regarding how the kinetic energy of a storm varies physically. As expected, IKE tends to increase with increasing lower-level vorticity and decreasing central pressure. However, the relationships between IKE and other metrics such as ocean thermodynamics and upper level winds can be more complex.

If there is a growing trend of intense TCs migrating northward over time, this could imply the potential for a corresponding growing trend in IKE across the North Atlantic, as IKE growth is promoted both when storms intensify and while storms move into the mid-latitudes. With all of the nonlinearities in the system, such as the fact that moderate shear can be both a hindrance and a supporting mechanism for storm growth, it may be difficult to estimate how IKE variability will change in a future climate, and future work is quite clearly needed. The over two decades of wind radii data for the North Atlantic with their associated uncertainties may be insufficient to conduct a rigorous trend analysis of IKE. However, statistical-

dynamical models like SPIKE2 can be integrated with model simulations of the future climate to better assess projected IKE changes in the future.

Beyond individual storms, IKE estimates can be aggregated into a seasonal metric, TIKE, which offers a unique evaluation of a season's activity level. TIKE is appealing because of its comprehensive nature to capture size, duration, intensity, and number of TCs in a particular season. Given a longer record of wind structure, these seasonal TIKE estimates can build upon the initial results presented here to better understand how climate cycles affect the interannual variability of more than just storm intensity and frequency.

Overall, the review above clearly shows that the studies on IKE are still in their infancy, and there is yet a lot to be understood and derived from them. Much of the current work is focused in utilizing IKE for operational use. In the meanwhile, the community would be well served to pursue further progress in understanding and predicting the variability of IKE and the overall TC wind field structure, given the significance of both storm size and intensity to hurricane damage. More specifically, model- and observationally-based case studies specifically focused on IKE and storm structure would be helpful to better understand how storm-specific dynamics and environmental forcings modulate IKE during the lifetime of a TC. On longer timescales, additional research clearly is needed to better understand historical interannual and multi-decadal IKE variability, since most of the work presented here is limited to just the past 20–30 years. By understanding the long-term historical trends, and by improving future climate projections, it should be possible to better understand how IKE might vary in a future climate. Finally, as mentioned earlier in this section, nearly all of the research on IKE is limited to the North Atlantic. As data quality and coverage improves around the globe, studies should expand to other basins to get a more comprehensive global perspective on IKE and its variability.

Acknowledgements We thank Drs. Frank Marks, Jonathan Vigh, and the editorial staff for their very useful reviews and comments on an earlier version of this chapter. Sections of this chapter are adapted from the Ph. D. dissertation of the first author. Thanks are also due to Drs. Robert Hart, Mark Powell, Phillip Sura, Allan Clarke, Ming Ye, and Mark Bourassa for their helpful comments and feedback. This work was supported by grants from NOAA (NA12OAR4310078) USGS (USGSG13AC00408), and South Florida Water Management District (PO 039231).

References

Atlas R, Hoffman RN, Ardizzone J, Leidner SM, Jusem JC, Smith DK, Gombos D (2011) A cross-calibrated, multiplatform ocean surface wind velocity product for meteorological and oceanographic applications. Bull Am Meteorol Soc 92:157–174. https://doi.org/10.1175/2010BAMS2946.1

Baldini LM et al (2016) Persistent northward North Atlantic tropical cyclone track migration over the past five centuries. Sci Rep 6:37522. https://doi.org/10.1038/srep37522

Bove MC, Elsner JB, Landsea CW, Niu X, O'Brien JJ (1998) Effects of El Niño on U.S. landfalling hurricanes, revisited. Bull Am Meteorol Soc 79:2477–2482. https://doi.org/10.1175/1520-0477(1998)079<2477:EOENOO>2.0.CO;2

Brennan MJ, Hennon CC, Knabb RD (2009) The operational use of QuikSCAT ocean surface vector winds at the National Hurricane Center. Weather Forecast 24:621–645. https://doi.org/10.1175/2008WAF2222188.1

Buchanan S, Misra V, Bhardwaj A (2018) Integrated kinetic energy of Atlantic tropical cyclones in a global ocean surface wind analysis. Int J Climatol 38:2651–2661. https://doi.org/10.1002/joc.5450

Cangialosi JP, Landsea CW (2016) An examination of model and official national hurricane center tropical cyclone size forecasts. Weather Forecast 31:1293–1300

Colbert AJ, Soden BJ (2012) Climatological variations in North Atlantic tropical cyclone tracks. J Clim 25:657–673. https://doi.org/10.1175/JCLI-D-11-00034.1

Crosset KM, Culliton TJ, Wiley PC, Goodspeed TR (2004) Population trends along the coastal United States: 1980–2008. National Oceanic and Atmospheric Administration, Silver Spring, p 47 https://aamboceanservice.blob.core.windows.net/oceanserviceprod/programs/mb/pdfs/coastal_pop_trends_complete.pdf

Dean L, Emanuel KA, Chavas DR (2009) On the size distribution of Atlantic tropical cyclones. Geophys Res Lett 36:L14803

DeMaria M, Kaplan J (1999) An updated statistical hurricane intensity prediction scheme (SHIPS) for the Atlantic and eastern north Pacific basins. Weather Forecast 14:326–337

Demuth J, DeMaria M, Knaff JA, Vonder Haar TH (2004) Validation of an Advanced Microwave Sounder Unit (AMSU) tropical cyclone intensity and size estimation algorithm. J Appl Meteorol Climatol 43:282–296. https://doi.org/10.1175/1520-0450(2004)043,0282:EOAMSU.2.0.CO;2

Demuth J, DeMaria M, Knaff JA (2006) Improvement of advanced microwave sounding unit tropical cyclone intensity and size estimation algorithms. J Appl Meteorol Climatol 45:1573–1581. https://doi.org/10.1175/JAM2429.1

Emanuel K (2005) Increasing destructiveness of tropical cyclones over the past 30 years. Nature 436:686–688

Emanuel K (2007) Environmental factors affecting tropical cyclone power dissipation. J Clim 20:5497–5509

Evans C, Hart RE (2008) Analysis of the wind field evolution associated with the extratropical Transition of Bonnie (1998). Mon Weather Rev 136:2047–2065

Hamill TM, Bates GT, Whitaker JS, Murray DR, Fiorino MI, Galarneau TJ, Zhu Y, Lapenta W (2013) NOAA's second-generation global medium-range ensemble reforecast dataset. Bull Am Meteorol Soc 94:1553–1565

Holmlund K, Velden C, Rohn M (2001) Enhanced automated quality control applied to high-density satellite derived winds. Mon Weather Rev 129:517–529. https://doi.org/10.1175/1520-0493(2001)129,0517:EAQCAT.2.0.CO;2

Irish JL, Resio DT, Ratcliff JJ (2008) The influence of storm size on hurricane surge. J Phys Oceanogr 38:2003–2013

Ito R, Takemi T, Arakawa O (2016) A possible reduction in the severity of typhoon wind in the northern part of Japan under global warming: a case study. SOLA 12:100–105. https://doi.org/10.2151/sola.2016-023

Jarvinen BR, Neumann CJ, (1979) Statistical forecasts of tropical cyclone intensity for the North Atlantic basin. NOAA Tech Memo NWS NHC-10, 22 pp

Jarvinen BR, Neumann CJ, Davis MAS (1984) A tropical cyclone data tape for the North Atlantic Basin, 1886–1983: contents, limitations, and uses. NOAA Technical Memorandum NWS NHC 22, Coral Gables, 21 pp

Kantha L (2006) Time to replace the Saffir-Simpson hurricane scale? Eos Trans AGU 87(1):3. https://doi.org/10.1029/2006EO010003

Knaff JA, Zehr RM (2007) Reexamination of tropical cyclone wind-pressure relationships. Weather Forecast 22:71–88

Knaff JA, Slocum CJ, Musgrave KD, Sampson CR, Strahl B (2016) Using routinely available information to estimate tropical cyclone wind structure. Mon Weather Rev 144:1233–1247. https://doi.org/10.1175/MWR-D-15-0267.1

Kossin JP, Camargo SJ, Sitkowski M (2010) Climate modulation of North Atlantic hurricane tracks. J Clim 23:3057–3076. https://doi.org/10.1175/2010JCLI3497.1

Kossin JP, Emanuel KA, Vecchi GA (2014) The poleward migration of the location of tropical cyclone maximum intensity. Nature 509:349–352. https://doi.org/10.1038/nature13278
Kozar ME (2015) Analysis and prediction of integrated kinetic energy in Atlantic tropical cyclones. Dissertation, Florida State University
Kozar ME, Misra V (2014) Statistical prediction of integrated kinetic energy in North Atlantic Tropical cyclones. Mon Weather Rev 142:4646–4657. https://doi.org/10.1175/MWR-D-14-001117.1
Kozar ME, Misra V, Powell MD (2016) Hindcasts of integrated kinetic energy in Atlantic tropical cyclones: a neural network prediction scheme. Mon Weather Rev 144:4591–4602. https://doi.org/10.1175/MWR-D016-0030.1
Landsea CW, Franklin JL (2013) Atlantic hurricane database uncertainty and presentation of a new database format. Mon Weather Rev 141:3576–3592
Lucas C, Timbal B, Nguyen H (2014) The expanding tropics: a critical assessment of the observational and modeling studies. WIREs Clim Chang 5:89–112
Maclay KS, DeMaria M, Vonder Haar TH (2008) Tropical cyclone inner-core kinetic energy evolution. Mon Weather Rev 136:4882–4898
Manning DM, Hart RE (2007) Evolution of North Atlantic ERA40 tropical cyclone representation. Geophys Res Lett 34(5):L05705. https://doi.org/10.1029/2006GL028266
Misra V, DiNapoli S, Powell M (2013) The track integrated kinetic energy of Atlantic tropical cyclones. Mon Weather Rev 141:2383–2389
Moon I-J, Kim S-H, Klotzbach P, Chan JCL (2015) Roles of interbasin frequency changes in the poleward shifts of the maximum intensity location of tropical cyclones. Environ Res Lett 10:104004. https://doi.org/10.1088/1748-9326/10/10/104004
Morris M, Ruf CS (2016) Estimating tropical cyclone integrated kinetic energy with the CYGNSS satellite constellation. J Appl Meteorol Climatol 56:235–245. https://doi.org/10.1175/JAMC-D-16-0176.1
Murnane RJ, Elsner JB (2012) Maximum wind speeds and US hurricane losses. Geophys Res Lett 39:L16707. https://doi.org/10.1029/2012GL052740
Musgrave KD, Taft RK, Vigh JL, McNoldy BD, Schubert WH (2012) Time evolution of the intensity and size of tropical cyclones. J Adv Model Earth Syst 4:M08001
Pielke RA Jr, Landsea CW (1998) Normalized hurricane damages in the United States: 1925–1995. Weather Forecast 13(3):621–631. https://doi.org/10.1175/1520-0434(1998)013<0621:NHDITU>2.0.CO;2
Powell M, Kozar M, (2015) Tropical cyclone integrated kinetic energy in the Atlantic basin. 5th Int. Summit on Hurricanes and Clim Change, Crete, Greece, Aegean Conferences, 24
Powell MD, Reinhold TA (2007) Tropical cyclone destructive potential by integrated kinetic energy. Bull Am Meteorol Soc 88:513–526
Powell MD, Houston SH, Amat LR, Morisseau-Leroy N (1998) The HRD real-time hurricane wind analysis system. J Wind Eng Ind Aerodyn 77–78:53–64
Rappaport EN et al (2009) Advances and challenges at the National Hurricane Center. Weather Forecast 24:395–419. https://doi.org/10.1175/2008WAF2222128.1
Schenkel BA, Hart RE (2012) An examination of tropical cyclone position, intensity, and intensity life cycle within atmospheric reanalysis datasets. J Clim 25(10):3453–3475
Sitkowski M, Koss JP, Rozoff CM (2011) Intensity and structure changes during hurricane eyewall replacement cycles. Mon Weather Rev 139:3829–3847
Velden C et al (2005) Recent innovations in deriving tropospheric winds from meteorological satellites. Bull Am Meteorol Soc 86:205–223. https://doi.org/10.1175/BAMS-86-2-205
Vigh JL, Knaff JA, Schubert WH (2012) A climatology of hurricane eye formation. Mon Weather Rev 140:1405–1426. https://doi.org/10.1175/MWR-D-11-00108.1
Wang C, Enfield DB (2001) The tropical Western Hemisphere warm pool. Geophys Res Lett 28:1635–1638. https://doi.org/10.1029/2000GL011763

Wang C, Enfield DB, Lee S-K, Landsea CW (2006) Influences of the Atlantic warm pool on Western Hemisphere summer rainfall and Atlantic hurricanes. J Clim 19:3011–3028. https://doi.org/10.1175/JCLI3770.1

Wang C, Liu H, Lee S-K, Atlas R (2011) Impact of the Atlantic warm pool on United States landfalling hurricanes. Geophys Res Lett 38:1635–1638. https://doi.org/10.1029/2011GL049265

Weissman DE, Stiles BW, Hristova-Veleva SM, Long DG, Smith DK, Hilburn KA, Jones WL (2012) Challenges to satellite sensors of ocean winds: addressing precipitation effects. J Atmos Ocean Technol 29:356–374. https://doi.org/10.1175/JTECH-D-11-00054.1

World Meteorological Organization (1970) The Beaufort Scale of wind force. WMO Commission for Maritime Meteorology, Marine Sciences Affairs Report No. 3, WMO, 22 pp

Yu J-Y, Chiu P-G (2012) Contrasting various metrics for measuring tropical cyclone activity. Terr Atmos Ocean Sci 23:303–316

Yu J–Y, Chou C, Chiu P-G (2009) A revised accumulated cyclone energy index. Geophys Res Lett 36:L14710. https://doi.org/10.1029/2009GL039254

Zhai AR, Jiang JH (2014) Dependence of US hurricane economic loss on maximum wind speed and storm size. Environ Res Lett 9. https://doi.org/10.1088/1748-9326/9/6/064019